ELSEVIER

Contents lists available at ScienceDirect

Journal of the Neurological Sciences

journal homepage: www.elsevier.com/locate/jns





Longitudinal evolution of diffusion metrices within the Cerebello-Thalamo-cortical tract after MRgFUS thalamotomy for essential tremor

Neeraj Upadhyay ^{a,b,*}, Marcel Daamen ^a, Veronika Purrer ^{b,c}, Valeri Borger ^d, Carsten Schmeel ^e, Jonas Krauss ^a, Angelika Maurer ^a, Alexander Radbruch ^{b,e}, Ullrich Wüllner ^c, Henning Boecker ^{a,b}

- ^a Clinical Functional Imaging group, Department of Nuclear Medicine, University Hospital Bonn, Bonn, Germany
- b German Center for Neurodegenerative Diseases (DZNE) Bonn, Bonn, Germany
- ^c Clinic for Parkinson's, Sleep and Movement Disorders, University Hospital Bonn, Bonn, Germany
- ^d Department for Neurosurgery, University Hospital Bonn, Bonn, Germany
- e Department for Neuroradiology, University Hospital Bonn, Bonn, Germany

ARTICLE INFO

Keywords: Essential tremor MRgFUS Fractional anisotropy Cerebello-thalamo-cortical tract Axial diffusivity Mean diffusivity Outcome

ABSTRACT

Magnetic resonance-guided focused ultrasound (MRgFUS) thalamotomy in essential tremor (ET) targets ventral intermediate nucleus hub region within cerebello-thalamo-cortical tract (CTCT). Understanding the microstructural changes in CTCT over time and their link to tremor improvement is crucial from a tremor-network perspective. We retrospectively analyzed tremor scores, lesion characteristics, and diffusion MRI-derived CTCT microstructural measures in 27 ET patient's pre-treatment (T0), at 1 month (T2), and 6 months (T3) post-MRgFUS. Using probabilistic tractography, we created an average CTCT mask at T0 for assessing fractional anisotropy (FA), axial (AD), mean (MD), and radial diffusivity (RD) measures across time points. Significant tremor reduction was observed at T2 and T3. The Linear mixed effect analyses showed significant time effects for FA, MD, and AD. Relative to baseline, post-hoc comparisons showed a significant decrease of FA and AD at lesion site only for T2. Instead, there was a significant increase in AD and MD at T3 compared to T2 at lesion site, and remotely near the motor cortex. Lesion size and FA changes in the CTCT at T2 showed only trend-level correlations with tremor outcome. Stronger associations were observed for the thalamic lesion-tract overlap at T2, which were even more robust at T3. Dynamic microstructural changes suggest early axonal disruption at the lesion site and subsequent reorganization, with remote CTCT changes potentially indicating chronic degeneration. Meanwhile, microstructural measures show limited predictive value for tremor outcome at 6 months compared with macroanatomical lesion-CTCT overlap. Yet, advanced diffusion imaging protocol could increase the sensitivity to predict MRgFUS clinical outcome.

1. Introduction

Essential tremor (ET) is a common movement disorder [1] and has recently been recognized as the most common form of cerebellar degeneration [2]. The pathophysiology of ET involves rhythmic oscillations that propagate from the cerebellum via the ventral intermediate nucleus (VIM) of the thalamus along the cerebello-thalamo-cortical tract

(CTCT) to motor cortical areas [3-5].

Neuromodulation methods like deep brain stimulation (DBS) and magnetic resonance-guided focused ultrasound (MRgFUS) [6,7] have been reported as effective treatments to alleviate drug-resistant tremor in ET ([8–10]; W. K. [11]). The VIM serves as a key therapeutic target for both neuromodulation methods in ET [12]. In particular, MRgFUS creates a permanent focal brain lesion in the VIM by applying thermal

Abbreviations: MRgFUS, Magnetic Resonance Guided Focused Ultrasound; ET, Essential Tremor; VIM, Vental intermediate nucleus; CTCT, cerebello-thalamocortical tract; T0, Before MRgFUS; T2, 1 month after MRgFUS; T3, 6 months after MRgFUS; CRST, Clinical rating scores for tremor; DWI, Diffusion Weighted Imaging; FA, Fractional Anisotropy; AD, Axial Diffusivity; MD, Mean Diffusivity.

^{*} Corresponding author at: Clinical Functional Imaging Group, Department of Nuclear Medicine, University Hospital Bonn, Bonn, Germany. E-mail address: Neeraj.Upadhyay@ukbonn.de (N. Upadhyay).

ablation via focused ultrasound [13]. The localized tissue damage at the lesion may trigger chronic fiber degeneration and/or fiber rearrangements within the CTCT, both locally and distantly from the lesion [14–18]. Understanding the dynamics of microstructural alterations in the CTCT resulting from MRgFUS thalamotomy is essential to determine their impact on treatment outcomes and the nature of any ensuing degeneration and reorganization.

The amount of overlap of the lesion extent with the CTCT tract is suggested to be related to clinical tremor improvement [19,20]. Beyond lesion volume, advanced neuroimaging techniques, such as diffusionweighted imaging (DWI), have been used to target CTCT in ET [21-23] and to assess white matter (WM) microstructural changes due to MRgFUS thalamotomy [24,25]. Decreased fractional anisotropy (FA) and increased mean diffusivity (MD) provide information about the loss of microstructural integrity [26]. Axial diffusivity (AD) and radial diffusivity (RD) can provide additional information on axonal damage or demyelination, respectively [27,28]. While the specificity of these measures in identifying pathology is still debated [29], AD and RD provide sensitive indicators for microstructural alterations after treatment [30]. Recent studies have reported microstructural alterations in the CTCT associated with tremor reduction [11,16,19]. Relative local decreases in FA in the targeted VIM have been linked to tremor improvement [16,18,24,31] within a 3- to 6-month duration following MRgFUS in ET. Moreover, local and distant increases in AD and RD along the CTCT have been reported over follow-up periods of three months [14,15]. Even one year after MRgFUS thalamotomy, decreases in FA and increases in MD and RD were reported, both locally and remotely [16]. These studies shed light on potential underlying mechanisms of tract reorganization, notably axonal damage or reorganization and demyelination.

However, these studies frequently have relatively small sample sizes [16,17,24]. Regarding the clinical significance of the observed changes, existing studies also demonstrate inconsistencies when correlating acute microstructural changes (1–3 days post-MRgFUS) with long-term clinical outcomes [15,16,18,24]. These are possibly due to the influence of local edema, compromising the specificity of the microstructural measures. Therefore, it is crucial to assess the relationship between microstructural measures and clinical outcomes when edema is largely regressed to gain more accurate insights. Finally, the intermediate evolution of diffusion metrics following MRgFUS lesioning is limited by the fact that many publications to date either do not include DWI measurements after three months of intervention [14,15,31] or, on the other hand, only focus on long-term outcomes after one year [16,24].

In the present study, we examined a comparatively large cohort of ET patients including intermediate time points i.e., before, one month, and six months after MRgFUS thalamotomy, to assess both, one- and sixmonths intervention effects on voxel-wise DWI measures of microstructural integrity within the CTCT, both in the treated and untreated (for control) hemisphere to validate earlier findings showing one- and six-months follow-up diffusion changes. We hypothesized that 1) while microstructural changes occur at the lesion site are still detectable after one-month recovery following MRgFUS, additional remote changes along the CTCT tract will only manifest during six-months follow-up. Moreover, we assessed 2) whether the observed lesion-specific and remote alterations in DWI microstructural measures were associated with the amount of tremor reduction at one- and six months, respectively. For comparison, we also 3) examined the relationship of clinical outcome with two macroanatomical imaging measures: the overall lesion volume and the overlap between the lesion and CTCT.

2. Methods

Twenty-seven patients (23 right-hand and 4 left-hand dominant) with severe drug-refractory ET (defined as at least two insufficient prior medication treatments) received unilateral MRgFUS treatment between October 2018 and October 2023. According to the MDS consensus

criteria [32], a neurologist with expertise in movement disorders verified the ET diagnosis. Exclusion criteria included brain injury, epilepsy, coagulopathies, severe heart disease, a history of psychiatric illnesses or substance abuse, cognitive impairment, and a skull density ratio below 0.3, as this influences the MRgFUS treatment accuracy. The details of inclusion criteria for MRgFUS are provided in the German Clinical Trials registry (DRKS00016695).

The Institutional Review Board (Ethikkommission an der Medizinischen Fakultät Bonn) gave their approval (Ethics no. 314/18), and the study was carried out in accordance with the Declaration of Helsinki. Every Participant provided informed written consent before inclusion.

The detailed protocol for MRgFUS treatment has been described previously [20,33,34]. In brief, the patient's head was fixed in a stereotactic frame in the focused ultrasound system (ExAblate 4000 System, InSightec, Haifa, Israel) while the procedure was carried out in a 3-Tesla (3 T) MRI system (Discovery MR750w, GE Healthcare, Chicago, IL, USA). The thalamic VIM contralateral to the hand most affected by tremor was chosen as target. The standard stereotactic coordinates used for the VIM were 14 mm lateral to the midline or 11 mm lateral to the wall of the third ventricle and 25 % anterior to the posterior commissure along the intercommissural line. Subtle adaptations of the target coordinates were made according to intraoperative clinical assessments regarding optimal tremor reductions, side effects, and pre-treatment DTI assessments of CTCT coordinates, as well as medial lemniscus and corticospinal tracts. Finally, a permanent lesion was produced (temperature range of 55 to 60 °C) using multiple sonications at sufficient energy levels.

2.1. Clinical evaluation

Clinical evaluations were carried out by two trained neurologists two days before (T0), as well as three days (T1), one month (T2), and six months (T3) after MRgFUS treatment. The assessment included the Fahn and Tolosa Clinical Rating Scale for Tremor (CRST) [35], which is frequently used as a severity score in the clinical evaluation of ET [36]: A modified composite (CRST-AB) including seven items was assembled from its subscale B and the upper extremity tremor items of subscale A. Greater tremor severity was indicated by higher CRST-AB scores (maximum: 28). We calculated separate CRST-AB scores for both, the treated and the untreated side.

2.2. MRI acquisition

MRI was obtained at T0, T1, T2, and T3 following MRgFUS therapy using a 3 T scanner (Philips Achieva TX, Best, The Netherlands) equipped with an eight-channel SENSE (SENSitivity Encoding) head coil. The protocol included 3D T1-weighted magnetization-prepared rapid gradient echo (MPRAGE) sequences (TR = 7.294 ms, TE = 3.93 ms, flip angle =15°, parallel imaging with SENSE factor = 2; 180 sagittal slices with 1 mm thickness; field of view (FOV) = 256×256 mm, matrix = 256×256 , reconstructed voxel size = 1x1x1 mm³; total scan time = 279.6 s), as well as DWI using single-shot spin-echo echo-planar imaging (TR = 8867 ms, TE = 67 ms, flip angle = 90° , SENSE factor = 2.4; 70 axial 2-mm slices (no gap), FOV = 224×224 mm, matrix = 112×112 , reconstructed voxel size = 2x2x2 mm³), acquiring 56 gradient directions with b = 1200 s/mm2, and 6 interspersed B0 maps.

2.3. MR data processing

2.3.1. Lesion volume segmentation

Due to the presence of local edema, which is a temporary phenomenon [33], we didn't use the data immediately following MRgFUS treatment (T1) in our analysis. At T2 and T3, T1-weighted images were used to create the lesion ROI's in each individual and then assessed the lesion volume. One rater (VP) manually delineated the lesions in each individual at each time point using the 3D editing tool in ITK-SNAP

(version 3.6.0; https://www.itk-snap.org/) and calculated the lesion volume by obtaining their 3D native space volumes in mm³.

2.3.2. Lesion-CTCT overlap

To derive a tract-specific estimate of lesion extent, the individual overlap was calculated between lesions from T2 and T3 and CTCT. For this purpose, the manually segmented lesions at T2 and T3 were transformed to T0. The overlap between the CTCT and the binary lesion was calculated using the following formula [37]:

$$\textit{Lesion CTCT overlap} = 1 - \left(\frac{\textit{tract}_{\textit{area}} - \textit{intersect}_{\textit{area}}}{\textit{tract}_{\textit{area}}}\right)$$

where $intersect_{area}$ is the overlap between the tract and the lesion in the same slice, and $tract_{area}$ is the area of the tract that corresponds to the maximal extent of the lesion, represented in the number of pixels.

2.3.3. Microstructural parameters

DWI data from T0, T2, and T3 were analyzed using FDT toolbox (htt ps://fsl.fmrib.ox.ac.uk/fsl/fslwiki/FDT) available in FSL-6.04. The preprocessing pipeline included susceptibility distortion, motion, and eddy current correction. Susceptibility distortion correction was carried out using the opposite phase encoding non-diffusion (b0) image by applying the top-up tool. Later, the susceptibility distortion parameters were inserted in the eddy tool in order to correct for susceptibility, motion, and eddy currents in a single step. This step also produced the vector direction after correcting for rotation. The eddy current-corrected diffusion data and the rotated vectors were used to estimate the fiber orientation using the bedpostX tool. The output was used to perform the probabilistic tractography.

Probabilistic tractography was performed to estimate the location of the CTCT at T0 using the ipsilateral dentate nucleus as seed region and passing through the ipsilateral superior cerebellar peduncle (SCP), the contralateral thalamus and the contralateral precentral gyrus (selected due to the treatment of tremor in upper extremities) as wavpoints in reference to the treated side. Seeds and waypoints were extracted from standard atlases: dentate nucleus [38], SCP (ICBM-DTI-81 white-matter labels atlas [39], thalamus (individual space parcellation using the model-based segmentation tool FSL first; https://fsl.fmrib.ox.ac.uk/fs 1/fslwiki/FIRST), and precentral gyrus (Harvard-Oxford cortical atlas in the MNI 1 mm space). All the atlas-based regions of interest were nonlinearly registered to the individual space. Later, a linear rigid transformation was applied to bring the seed and waypoints into diffusion space. For tractography, 5000 streamlines were generated from the seed region using the standard parameters of the Probtracx2 function in the FDT toolbox.

A probabilistic map was obtained with a value assigned to each brain voxel that indicated the total number of streamlines that travelled from the "seed" region through that voxel to the "target" region. The map was strictly thresholded to keep only voxels where at least 5 % of all streamlines from the seed region made it to the target region (also known as the "waytotal" number) in order to improve the findings. Further, to assess the diffusion metrices within CTCT, we nonlinearly registered the individual tracts to the MNI ICBM 152 non-linear 6th Generation Symmetric atlas, available in FSL [40]. Finally, we created common CTCT mask in standard MNI space by averaging the above probabilistic maps in standard space from each individual before MRgFUS (T0) and thresholding to 1 % of the averaged streamline density to create anatomically accurate tract (visually inspected by a neurologist (VP).

To construct the diffusion metrics, we used the weighted least square fitting approach and created FA, AD, RD, and mean diffusivity (MD) maps to evaluate the microstructural changes from T0 to T2, T0 to T3 and T2 to T3. In three subjects, the diffusion maps were flipped from right to left to bring the MRgFUS thalamotomy sites to the same side and to allow group statistical comparisons. Later, the respective FA, AD, RD,

and MD maps were nonlinearly registered to the above mentioned MNI ICBM 152 atlas space. Further, we implemented a 5 mm full width half maximum (FWHM) Gaussian kernel to smooth the data.

2.4. Statistics

Clinical CRST-AB scores, lesion volumes and lesion-CTCT overlap were analyzed using Jamovi (version: 2.3.28.0; https://www.jamovi.org). We performed a repeated measures ANOVA to compare CRST-AB scores at different time points for both, treated and nontreated sides. For lesion volume and lesion-CTCT overlap pairwise comparisons between T2 and T3 were performed. Significant results were reported at p < 0.05, after implementing the multiple comparison correction for posthoc testing. Effect sizes were reported as eta squared (η^2) value for the F-test and as Cohen's d (d) for the t-statistics.

To assess the microstructural changes within the CTCT over time, we performed linear mixed effect (LME) modeling using the 3dLmer tool from AFNI (https://afni.nimh.nih.gov/pub/dist/doc/program_help/3d LMEr.html). A simple model was created including time as a fixed effect and subjects as a random effect within the CTCT mask. This produces main effects of time and post-hoc pairwise comparisons between implemented contrast to assess the direction of changes between T0, T2, and T3. Based on a cluster-defining height threshold of p < 0.001 (voxelwise), we implemented multiple comparison correction using the updated AutoCorrelation Function (ACF) approach to calculate the amount of smoothing and applied a simulation approach to identify clusters surviving family-wise error (FWE) correction at $\alpha < 0.05$ with corresponding cluster size (k). Furthermore, we corrected the post-hoc comparisons by adjusting for the number of comparisons ($\alpha = 0.0166$ (0.05/3)) and represented results with corresponding cluster sizes.

To explore the clinical relevance of the observed microstructural changes after lesioning, we performed correlation analyses between the percent change in CRST-AB tremor scores and imaging parameters, including (A) global lesion volume [41] and (B) the lesion-CTCT overlap, which were already examined in earlier studies [42], as well as (C) the relative diffusion metric changes obtained from significant clusters in our DWI analyses. We employed Kendall's tau-b (τ) rank-based correlation [43] due to its higher accuracy in calculating p-values for smaller sample sizes and its robustness against data discrepancies [44]. Significant correlations were reported at p < 0.05.

3. Results

3.1. Clinical scores

All demographic and clinical measures are provided in Table 1. Repeated measures ANOVA for the treated side showed significant changes in CRST AB subscale over time after correcting for sphericity using the Greenhouse-Geisser method (F(1.6) = 154, $p < 0.001, \, \eta^2 = 0.682$) (Fig. 1A). Post-hoc comparisons indicated a significant reduction for CRST-AB at T2 (M \pm SD = 5.07 ± 4.27 ; t(26) = $-13.7, \, p < 0.001, \, d = -2.649$) compared to T0 (M \pm SD = 18.78 ± 4.27). The CRST-AB remained reduced at T3 relative to T0 (M \pm SD = 5.85 ± 4.56 ; t(26) = $-13.43, \, p < 0.001, \, d = -2.585$). No significant differences were observed in CRST-AB between T2 and T3 (t(26) = $-1.25, p = 0.437, \, d = -0.240$). Repeated measures ANOVA for the untreated side showed no significant changes in CRST-AB over the time (F(2) = $0.316, \, p = 0.730, \, \eta^2 = 0.002$) (Fig. 1B).

3.2. Lesion volume segmentations

Pairwise comparisons showed a significantly (t(26) = 8.39, p < 0.001, d = 1.61) reduced lesion volume at T3 (M \pm SD = 30.9 \pm 33.9 mm³) compared to T2 (M \pm SD = 109 \pm 62.8 mm³) (Fig. 1C).

Table 1Clinical and demographic data of 27 Essential Tremor patients.

SUB_ID	Age range (years)	Gender (M/F)	CRST-subscale AB						Lesion size (mm3)	
			TO		T2		T3		1-month	6-months
			T	NT	T	NT	T	NT		
SUB_001	60's	F	19	21	4	18	3	15	97	34
SUB_002	60's	M	14	12	2	10	2	10	92	10
SUB_003	70's	M	24	24	9	21	10	17	119	65
SUB_004	60's	M	17	8	7	3	3	5	39	18
SUB_005	70's	F	22	22	24	21	21	24	0	0
SUB_006	60's	M	16	9	3	12	3	10	68	28
SUB_007	60's	M	16	18	3	17	4	20	73	17
SUB_008	80's	M	18	17	4	14	5	12	56	12
SUB_009	60's	M	19	16	5	11	6	12	127	24
SUB_010	70's	M	24	23	3	20	11	23	109	24
SUB_011	80's	F	19	16	6	13	17	17	129	37
SUB_012	70's	M	23	25	5	22	4	26	74	16
SUB_013	80's	M	13	16	2	17	4	20	280	180
SUB_014	30's	M	14	9	1	7	3	9	195	45
SUB_015	50's	M	20	21	4	22	5	22	123	77
SUB_016	70's	F	19	18	3	16	7	17	67	16
SUB_017	50's	M	13	12	4	15	3	15	144	23
SUB_018	80's	M	13	14	6	15	6	13	37	19
SUB_019	80's	M	25	18	3	16	2	15	100	20
SUB_020	80's	F	26	22	4	21	4	19	87	17
SUB_021	70's	M	14	14	2	18	2	12	231	32
SUB 022	70's	M	16	14	6	25	2	23	188	22
SUB_023	50's	M	24	24	8	21	6	25	42	19
SUB_024	70's	M	26	21	5	20	10	27	181	19
SUB_025	60's	F	14	21	7	24	7	26	76	16
SUB_026	60's	F	20	15	5	23	5	22	114	14
SUB 027	60's	F	19	8	2	5	3	5	96	31

Here, MRgFUS = magnetic resonance guided focused ultrasound, T0 = before MRgFUS, T2 = 1 month after MRgFUS, T3 = 6 months after MRgFUS, M = male, F = female, T = Treated and NT = non-treated side.

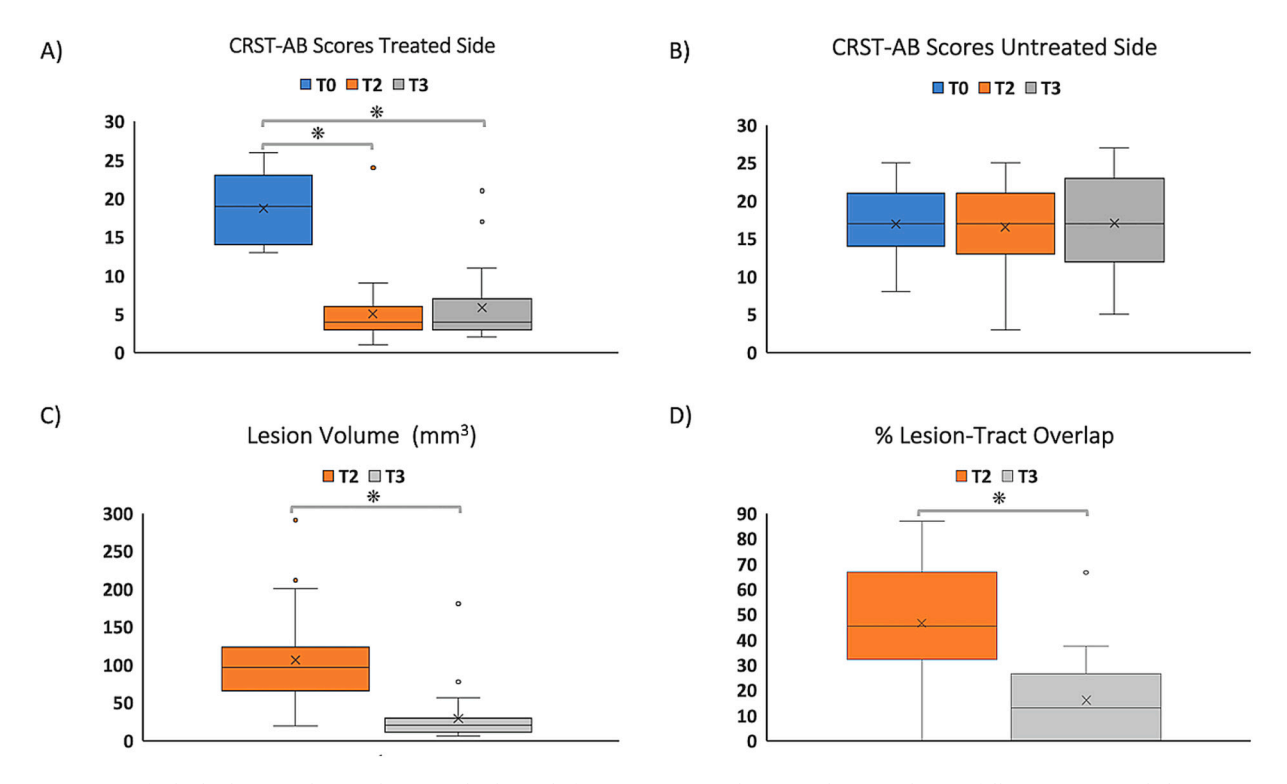


Fig. 1. Tremor scores for both, the treated (A) and untreated side (B), before (T0), one month (T2), and six months (T3) following MRgFUS thalamotomy; C) Lesion volume and (D) lesion-CTCT overlap at T2 and T3 following MRgFUS thalamotomy. *p < 0.001.

3.3. Lesion-CTCT overlap

We observed 46.5 % (range: 0–87 %) lesion-CTCT overlap at T2 which dropped to 16.1 % (0–66. 7 %) at T3 (t(26) = 7.50, p < 0.001, d = 1.44).

3.4. Microstructural changes within the CTCT

LME models showed significant effects of time at the thalamic lesion site for FA $(p<0.001,\,\alpha<0.05,\,k=132),$ AD $(p<0.001,\,\alpha<0.05,\,k=909),$ and MD $(p<0.001,\,\alpha<0.05,\,k=335)$ (Fig. 2: Supplementary Fig. 1 for corresponding box plots), but not RD. Post-hoc comparisons at T2 showed a significant decrease in FA $(p<0.001,\,\alpha<0.0166,\,k=196)$ and AD $(p<0.001,\,\alpha<0.0166,\,k=723)$ at the lesion site compared to T0 baseline (Fig. 2). Meanwhile, no significant decreases relative to T0 were observed at T3. Instead, AD $(p<0.001,\,\alpha<0.0166,\,k=1250)$ and MD $(p<0.001,\,\alpha<0.0166,\,k=865)$ increased significantly at T3 compared to T2.

Similar increases of AD (p < 0.001, α < 0.0166, k=170) and MD (p < 0.001, α < 0.0166, k=184) for T3 relative to T2 were also found in a

distant part of the CTCT between thalamus and precentral gyrus (p < 0.016) (Fig. 2): For the respective comparison versus T0, the same region also showed a cluster (k = 132) with increased AD values at T3 (Fig. 2) which just missed the cluster extent threshold (p < 0.001, $\alpha < 0.0166$, k > 133).

Within the CTCT of the untreated hemisphere, no significant time effect was found for any of the DWI metrics.

3.5. Correlations

Higher overall lesion volume at T2 showed only a trend-level positive correlation ($\tau=0.244,p=0.076$) with stronger one-month tremor reduction at T2, as expressed by percent change in CRST-AB_{(T0-T2)/T0} (Fig. 3A), but not at with tremor reduction at T3 (CRST-AB_{(T0-T3)/T0}) ($\tau=0.14,p=0.31$). Lesion-CTCT overlap at T2 showed a marginally significant positive correlation with CRST-AB_{(T0-T2)/T0} ($\tau=0.26,p=0.06$), and significantly with six-months percent change in CRST-AB_{(T0-T3)/T0} ($\tau=0.331,p=0.017,$ Fig. 3B). Neither lesion size nor lesion-CTCT overlap at T3 correlated with the clinical tremor improvement.

Regarding the significant clusters derived for the main DWI analyses,

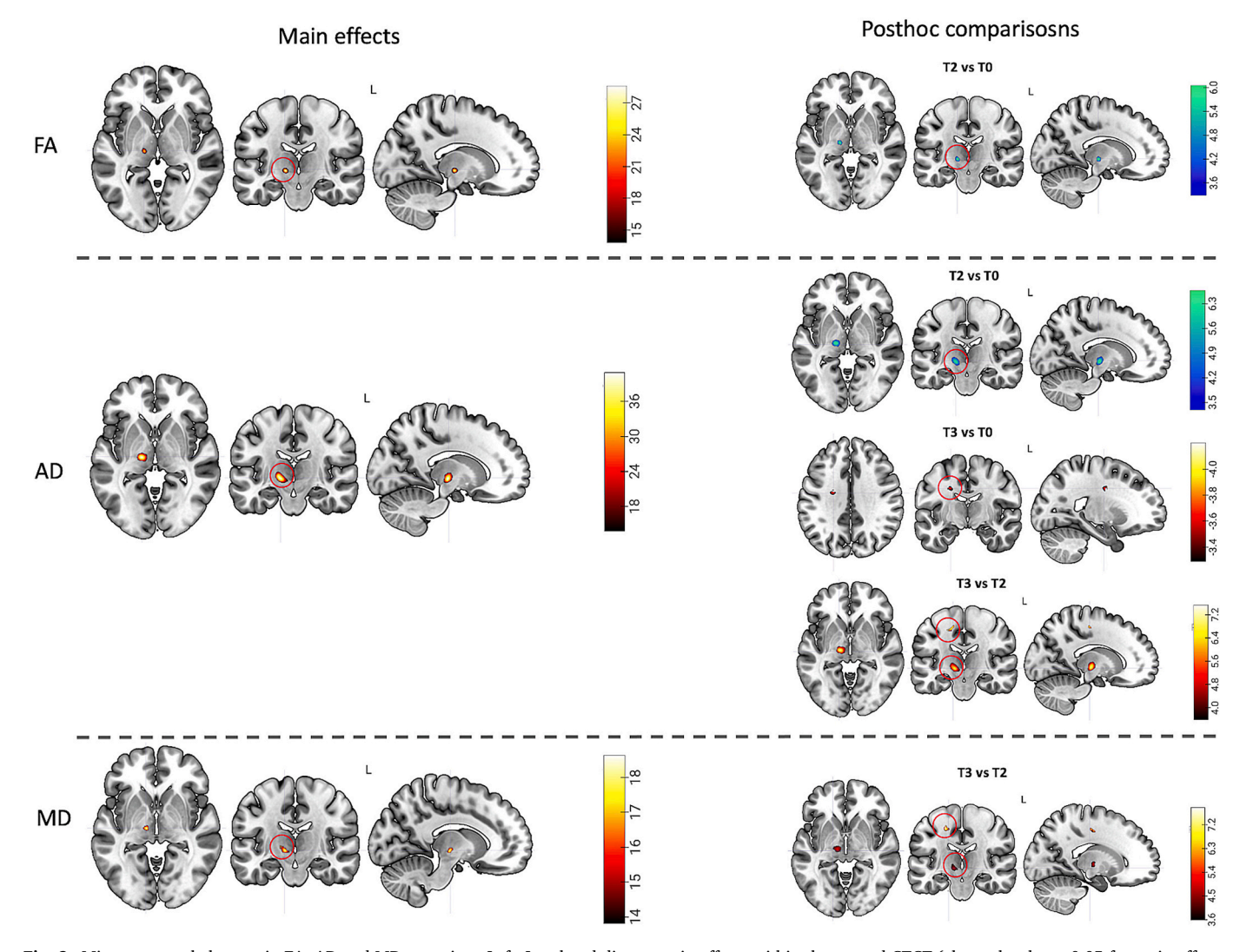


Fig. 2. Microstructural changes in FA, AD and MD over time. Left: Local and distant main effects within the treated CTCT (cluster-level $\alpha < 0.05$ for main effects, with cluster-defining height threshold p < 0.001 voxelwise). Right: Post-hoc contrasts corrected for multiple comparisons ($\alpha < 0.0166$: 0.05/3). To increase the visibility, we have highlighted (red circles) the significant clusters in the coronal plane. Color bars represent chi-square values for the ANOVA main effect and t-values for post-hoc comparisons (red-hot colors represents increases, blue-cool colors represent decreases). To = before MRgFUS, T2 = 1 month following MRgFUS, T3 = 6 months following MRgFUS, FA = fractional anisotropy, AD = axial diffusivity, and MD = mean diffusivity. (For interpretation of the references to color in this figure legend, the reader is referred to the web version of this article.)

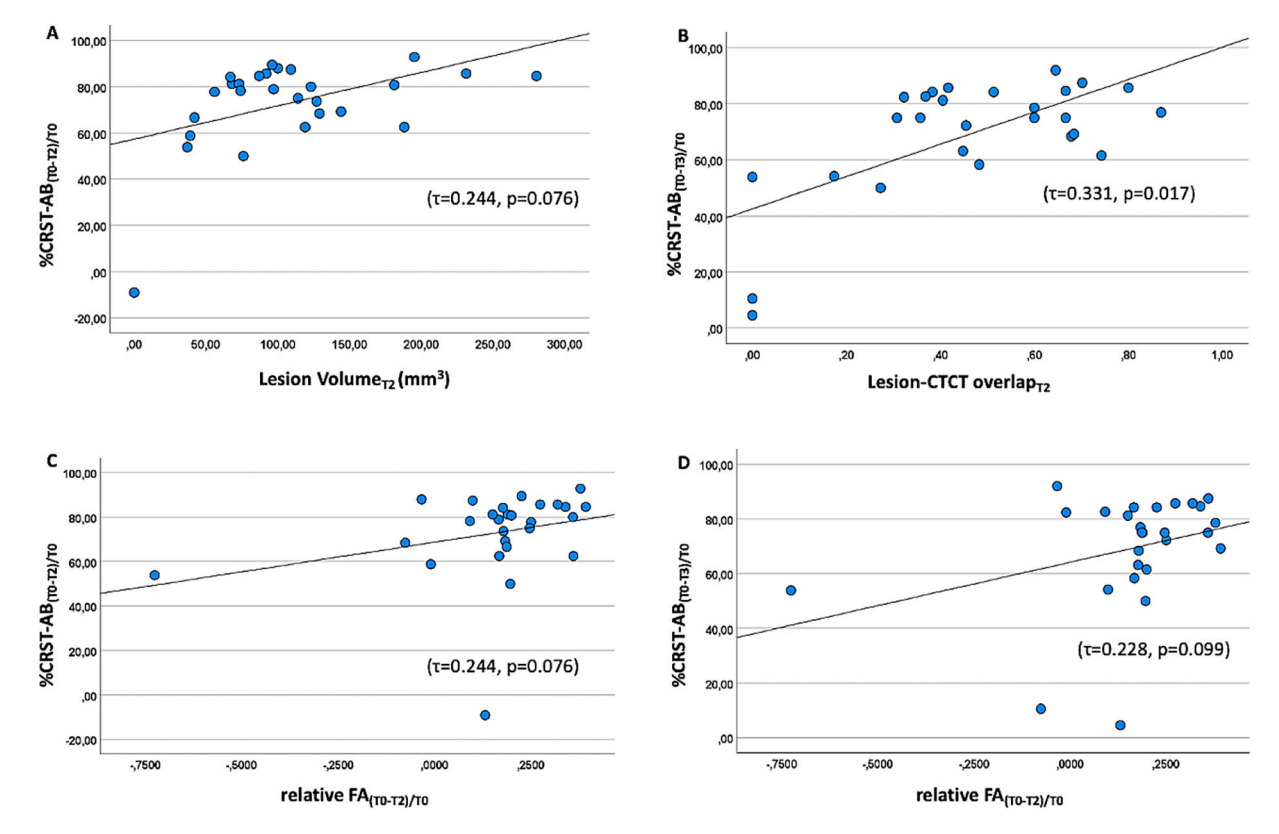


Fig. 3. Relationship between: A) lesion volume at 1 month (T2) correlates with percent CRST-AB, B) lesion-CTCT overlap at 1 month correlates with percent CRST-AB at 6 months (T3); relative FA changes at 1 month correlate with C) percent CRST-AB at 1 month and D) percent CRST-AB at 6 months. Trepresents the Kendall's rank correlation with the corresponding *p*-value. T0 = before MRgFUS, T2 = 1 month following MRgFUS, T3 = 6 months following MRgFUS, FA = fractional anisotropy, CTCT = cerebello-thalamo-cortical tract and CRST = Clinical Rating Scale for Tremor.

only at one month change in relative $FA_{(T0-T2)/T0}$ for the thalamic cluster showed trend-level positive correlations with the one-month percent change in CRST-AB $_{(T0-T2)/T0}$ ($\tau=0.244$, p=0.076, Fig. 3C) and sixmonths percent change in CRST-AB $_{(T0-T3)/T0}$ ($\tau=0.228$, p=0.099, Fig. 3D). No significant correlations were observed between the AD and MD changes for the distant CTCT cluster and clinical tremor improvement.

4. Discussion

To our knowledge, this is the first MRgFUS study in patients with severe pharmacoresistant ET which investigated longitudinal voxel-wise changes of microstructural integrity along the treated CTCT fiber tract beyond the first three months of intervention. Examining both one- and six months after treatment effects, the study provided further insights into the dynamics of the microstructural changes after MRgFUS. Apart from a significant and sustained reduction of tremor severity, and a strong decline in macroscopic lesion volume, microstructural changes in FA, AD, and MD were primarily observed at the lesion site, but also in a distant CTCT section of the treated hemisphere. These microstructural changes showed differential temporal dynamics over the 6-month time course: While FA at the thalamic lesion site showed a decrease at one month, but not at six months after MRgFUS treatment, AD presented an initial decrease followed by a subsequent increase after six months, which was paralleled by MD increases emerging after six months. Findings suggest some restitution of fiber organization in the damaged region, but no full recovery back to the original pre-intervention state. On the other hand, both AD and MD showed a delayed increase at six months (compared to one month after MRgFUS) in an upper aspect of the CTCT (between thalamus and precentral gyrus), which suggests sixmonths fiber changes beyond the original site of injury, possible due to chronic degeneration. Meanwhile, reductions in tremor severity were not associated with these distant changes, but only with lesion-specific imaging measures from the 1-month follow-up: Overall, the most robust association with six-months tremor reduction was observed between the percent overlap of the macroscopic lesion with the CTCT tract, even though FA changes showed a similar trend for both, one- and six-months follow-up outcomes.

The stable reductions in tremor severity at one and six months after unilateral MRgFUS treatment align with several recent studies [14–18,20,24,42]. Yet, the physiological substrates of these therapeutic effects, especially post-acute and longer-term structural and functional adaptations of the involved brain networks help to sustain tremor reduction, are only partially understood. Considering the ablation itself, lesion characteristics such as size and anatomical overlap with white matter tracts have been reported to relate to improvement in clinical tremor [20,42,45,46]. Similarly, we observed that after one month overall lesion volume marginally correlated with concurrent improvement in tremor severity, but it was not associated with tremor change after six months. Instead, a lesion-CTCT overlap metric was significantly correlated with six-months tremor improvement further validating the previous findings that the degree by which the lesion affects the CTCT is predicting long-term tremor improvement in ET ([19]; T. R. [16,46]).

Microstructural integrity can be altered due to pathology or treatment and characterized using diffusion measures [47]. Previous studies in ET patients have reported a decrease in FA locally at lesion location as well as remotely in cerebellar peduncle and between thalamus and motor cortex at longer-term following MRgFUS [14–16] suggesting that loss or increased incoherency of fibers leads to reduced microstructural integrity [48]. In line with these, we observed significant decreases in thalamic FA at one month following MRgFUS treatment, which at six months showed some evidence for recovery, as no significant difference from baseline was found here (Supplementary Fig. 1). Earlier study had reported significant FA decreases at three months [17], and there is

some evidence for incomplete recovery [18]. Meanwhile, Thaler et al. [16] reported FA decreases even after one year, but this could be due to larger residual lesions size (mean: $42.28 \pm 23.12 \, \mathrm{mm}^3$) after one year as compared to our study at only six months ($30.9 \pm 33.9 \, \mathrm{mm}^3$) which might reflect more extensive and sustained tissue loss in their patients. Concomitant with the FA changes, we observed a differential development of AD changes, an initial decrease at one month and an increase at six months. AD is thought to provide specific information about axonal injury or coherence in the absence of edema [30]. The one-month local decrease in AD is consistent with an animal study reporting an acute decrease in AD after MRgFUS due to axonal damage [48]. A residual influence of vasogenic edema should, however, not be discounted, also considering that AD levels increased to baseline levels at six months follow-up. Meanwhile, MD showed a relative increase from one month to six months, which may reflect chronic inflammatory processes [49].

Unlike previous studies [14-16], we did not observe remote FA changes. However, we obtained delayed increases in AD and MD in a distant region of the CTCT located below the motor cortex at six months, mainly compared to measurements at one month. These findings extend prior observations of AD or MD increase following three months [14] and even at one year [16] after MRgFUS. Although it is not clear whether MRgFUS lesion leads to axonal damage [48,50,51], a possibility of triggering a cascade of cellular and metabolic responses leading to Wallerian degeneration distal to the injury site still exists [52]. Accordingly, the remote MD increases found in our data and these previous studies would be consistent with this sort of protracted fiber loss, as increased MD is frequently interpreted to reflect reduced white matter integrity due to either axonal or myelin degradation [53]. Meanwhile, the colocalized increase of AD which was observed both in our data and Mazerolle et al. [14] would be more suggestive of regenerative processes, as higher AD would be interpreted to reflect higher axonal caliber or stronger coherent orientation of axons [54]. Given the ongoing debate about the specificity of these measures in identifying pathology, this cannot be clarified [29]. More generally, the distant changes showed no relationship with tremor reduction, thus, questioning the functional relevance of these distant AD and MD changes for the present clinical outcome.

Previous work has shown lesion FA values to correlate with tremor outcomes [18,24]. We only observed marginally significant associations between voxel-wise thalamic FA decrease and tremor reduction at one-and six-months following MRgFUS. There were also other studies that did not find significant associations between lesion-specific DWI metrics and clinical outcomes [15]. Methodological factors which vary between studies, including sample size, lesion volume, lesion-tract overlap, or variance of clinical outcomes, may contribute to the variability of these associations.

This study is not without limitations. The moderate sample size of this study limits generalizability and statistical power. Nevertheless, we were able to find significant microstructural changes in the targeted CTCT. The parameters of the DWI acquisition could be improved to attain higher spatial resolution, e.g., by using multi-shell acquisitions, in order to detect more subtle changes. We used a tractography-guided lesion approach, which accounts for individual anatomical variation, but may result in greater variability in lesion localization than an independent atlas-based method. By extending the number of longitudinal MR examinations, a more reliable estimation of the temporal trajectories of the observed changes would become possible. Finally, longer-term follow-ups (>1 year) that include clinical tremor scores and advanced MRI data analysis should better distinguish patients with stable outcomes from those with future symptom recurrences. These follow-ups should also increase predictability through microstructural changes. Moreover, clinical characterization could be augmented by objective measures (e.g., accelerometry).

5. Conclusion

This study further substantiates both one- and six months microstructural changes following unilateral MRgFUS in ET patients, as reported in prior studies with smaller cohorts, and often shorter followups. Beyond temporary reductions of diffusion MRI measures at the lesion site which were recurrent, and indicate axonal disruption or incoherency after MRgFUS in the first month, potentially followed by axonal reorganization in the six months, the present study also confirmed delayed microstructural changes in upper aspects of the CTCT which may reflect remote lesion effects on CTCT integrity, e.g., due to Wallerian-like degeneration. This warrants further validation with refined imaging protocols, especially to improve their limited potential as a predictive marker for treatment outcomes.

Author contribution

The MRgFUS study was conceptualised and designed by Henning Boecker and Ullrich Wüllner. Resources were largely provided by Carsten Schmeel, Alexander Radbruch, and Henning Boecker. Ullrich Wüllner, Veronika Purrer and Valeri Borger were involved in the MRgFUS treatment and other clinical aspects. The data analysis was carried out by Neeraj Upadhyay. Data curation was done by Neeraj Upadhyay, Veronika Purrer, and Jonas Krauß. Statistical analysis and interpretation of the data was carried out by Neeraj Upadhyay, Marcel Damen, and Henning Boecker. Neeraj Upadhyay, Angelika Maurer, Marcel Damen and Henning Boecker drafted and edited the manuscript. All authors critically reviewed and edited the manuscript and approved the final manuscript.

CRediT authorship contribution statement

Neeraj Upadhyay: Writing – review & editing, Writing – original draft, Visualization, Validation, Methodology, Investigation, Formal analysis, Data curation, Conceptualization. Marcel Daamen: Writing – review & editing, Validation, Methodology. Veronika Purrer: Writing – review & editing, Resources, Data curation. Valeri Borger: Project administration, Methodology, Data curation. Carsten Schmeel: Validation, Methodology, Investigation. Jonas Krauss: Writing – review & editing, Methodology, Data curation. Angelika Maurer: Writing – review & editing. Alexander Radbruch: Resources. Ullrich Wüllner: Writing – review & editing, Validation, Supervision, Methodology, Investigation, Funding acquisition, Conceptualization. Henning Boecker: Writing – review & editing, Writing – original draft, Validation, Supervision, Resources, Investigation, Funding acquisition, Conceptualization.

Funding

The MRgFUS system was in part funded by the German Research Foundation (INST 1172/644-1) and the University of Bonn's Faculty of Medicine.

Declaration of competing interest

Authors report no competing interest.

Acknowledgment

We acknowledge all the participants and their relatives for their support in carrying out this study. We also acknowledge the medical radiology assistants who performed the clinical data acquisition as well as the neurologists involved in clinical assessments.

Appendix A. Supplementary data

Supplementary data to this article can be found online at https://doi.org/10.1016/j.ins.2025.123604.

References

- [1] R.J. Elble, What is essential tremor? Curr. Neurol. Neurosci. Rep. 13 (6) (2013) 353, https://doi.org/10.1007/s11910-013-0353-4.
- [2] E.D. Louis, P.L. Faust, Essential tremor: the most common form of cerebellar degeneration? Cerebellum & Ataxias 7 (2020) 12, https://doi.org/10.1186/ s40673-020-00121-1.
- [3] R.C. Helmich, I. Toni, G. Deuschl, B.R. Bloem, The pathophysiology of essential tremor and Parkinson's tremor, Curr. Neurol. Neurosci. Rep. 13 (9) (2013) 378, https://doi.org/10.1007/s11910-013-0378-8.
- [4] A. Lenka, K.S. Bhalsing, R. Panda, K. Jhunjhunwala, R.M. Naduthota, J. Saini, R. D. Bharath, R. Yadav, P.K. Pal, Role of altered cerebello-thalamo-cortical network in the neurobiology of essential tremor, Neuroradiology 59 (2) (2017) 157–168, https://doi.org/10.1007/s00234-016-1771-1.
- [5] T. Welton, F. Cardoso, J.A. Carr, L.-L. Chan, G. Deuschl, J. Jankovic, E.-K. Tan, Essential tremor, Nat. Rev. Dis. Primers 7 (1) (2021) 83, https://doi.org/10.1038/ s41572-021-00314-w.
- [6] J. Germann, B. Santyr, A. Boutet, C. Sarica, C.T. Chow, G.J.B. Elias, A. Vetkas, A. Yang, M. Hodaie, A. Fasano, S.K. Kalia, M.L. Schwartz, A.M. Lozano, Comparative neural correlates of DBS and MRgFUS lesioning for tremor control in essential tremor, J. Neurol. Neurosurg. Psychiatry 95 (2) (2024) 180–183, https:// doi.org/10.1136/jnnp-2022-330795.
- [7] M. Giordano, V.M. Caccavella, I. Zaed, L. Foglia Manzillo, N. Montano, A. Olivi, F. M. Polli, Comparison between deep brain stimulation and magnetic resonance-guided focused ultrasound in the treatment of essential tremor: a systematic review and pooled analysis of functional outcomes, J. Neurol. Neurosurg. Psychiatry 91 (12) (2020) 1270–1278, https://doi.org/10.1136/jnnp-2020-323216
- [8] M. Agrawal, K. Garg, R. Samala, R. Rajan, V. Naik, M. Singh, Outcome and complications of MR guided focused ultrasound for essential tremor: a systematic review and meta-analysis, Front. Neurol. 12 (2021) 654711, https://doi.org/ 10.3389/fneur.2021.654711.
- [9] H. Ito, T. Shizuku, S. Aoki, S. Fukutake, T. Odo, K. Yamamoto, T. Yamaguchi, Magnetic resonance imaging-guided focused ultrasound thalamotomy for essential tremor patient with a clipped cerebral aneurysm and Alzheimer's disease: a case report, Neurol. Clin. Neurosci. 9 (4) (2021) 333–335, https://doi.org/10.1111/ pcp3_12507
- [10] A.M. Lak, D.J. Segar, N. McDannold, P.J. White, G.R. Cosgrove, Magnetic resonance image guided focused ultrasound thalamotomy. A single Center experience with 160 procedures, Front. Neurol. 13 (2022) 743649, https://doi. org/10.3389/fneur.2022.743649.
- [11] W.K. Miller, K.N. Becker, A.J. Caras, T.R. Mansour, M.T. Mays, M. Rashid, J. Schwalb, Magnetic resonance-guided focused ultrasound treatment for essential tremor shows sustained efficacy: a meta-analysis, Neurosurg. Rev. 45 (1) (2022) 533–544, https://doi.org/10.1007/s10143-021-01562-w.
- [12] M.N. Gallay, D. Jeanmonod, J. Liu, A. Morel, Human pallidothalamic and cerebellothalamic tracts: anatomical basis for functional stereotactic neurosurgery, Brain Struct. Funct. 212 (6) (2008) 443–463, https://doi.org/10.1007/s00429-007-0170-0
- [13] G.T. Haar, C. Coussios, High intensity focused ultrasound: physical principles and devices, Int. J. Hyperth. 23 (2) (2007) 89–104, https://doi.org/10.1080/ 02656730601186138
- [14] E.L. Mazerolle, R. Warwaruk-Rogers, P. Romo, T. Sankar, S. Scott, C.P. Rockel, S. Pichardo, D. Martino, Z.H.T. Kiss, G.B. Pike, Diffusion imaging changes in the treated tract following focused ultrasound thalamotomy for tremor, Neuroimage Rep. 1 (1) (2021) 100010, https://doi.org/10.1016/j.ynirp.2021.100010.
- [15] J.A. Pineda-Pardo, R. Martínez-Fernández, R. Rodríguez-Rojas, M. Del-Alamo, F. Hernández, G. Foffani, M. Dileone, J.U. Máñez-Miró, E. De Luis-Pastor, L. Vela, J.A. Obeso, Microstructural changes of the dentato-rubro-thalamic tract after transcranial MR guided focused ultrasound ablation of the posteroventral VIM in essential tremor, Hum. Brain Mapp. 40 (10) (2019) 2933–2942, https://doi.org/10.1002/bbm.24569
- [16] C. Thaler, Q. Tian, M. Wintermark, P. Ghanouni, C.H. Halpern, J.M. Henderson, R. D. Airan, M. Zeineh, M. Goubran, C. Leuze, J. Fiehler, K. Butts Pauly, J.A. McNab, Changes in the Cerebello-Thalamo-cortical network after magnetic resonance-guided focused ultrasound thalamotomy, Brain Connect. 13 (1) (2023) 28–38, https://doi.org/10.1089/brain.2021.0157.
- [17] M. Wintermark, J. Druzgal, D.S. Huss, M.A. Khaled, S. Monteith, P. Raghavan, T. Huerta, L.C. Schweickert, B. Burkholder, J.J. Loomba, E. Zadicario, Y. Qiao, B. Shah, J. Snell, M. Eames, R. Frysinger, N. Kassell, W.J. Elias, Imaging findings in MR imaging-guided focused ultrasound treatment for patients with essential tremor, AJNR Am. J. Neuroradiol. 35 (5) (2014) 891–896, https://doi.org/10.3174/ajnr.A3808.
- [18] G. Zur, O.H. Lesman-Segev, I. Schlesinger, D. Goldsher, A. Sinai, M. Zaaroor, Y. Assaf, A. Eran, I. Kahn, Tremor relief and structural integrity after MRI-guided focused US thalamotomy in tremor disorders, Radiology 294 (3) (2020) 676–685, https://doi.org/10.1148/radiol.2019191624.
- [19] J.L. Chazen, H. Sarva, P.E. Stieg, R.J. Min, D.J. Ballon, K.O. Pryor, P. M. Riegelhaupt, M.G. Kaplitt, Clinical improvement associated with targeted interruption of the cerebellothalamic tract following MR-guided focused

- ultrasound for essential tremor, J. Neurosurg. 129 (2) (2018) 315–323, https://doi.org/10.3171/2017.4.JNS162803.
- [20] V. Purrer, N. Upadhyay, V. Borger, C.C. Pieper, C. Kindler, S. Grötz, V.C. Keil, T. Stöcker, H. Boecker, U. Wüllner, Lesions of the cerebello-thalamic tract rather than the ventral intermediate nucleus determine the outcome of focused ultrasound therapy in essential tremor: a 3T and 7T MRI-study, Parkinsonism Relat. Disord. 91 (2021) 105–108, https://doi.org/10.1016/j. parkreldis.2021.09.013.
- [21] V. Krishna, F. Sammartino, R. Cosgrove, P. Ghanouni, M. Schwartz, R. Gwinn, H. Eisenberg, P. Fishman, J.W. Chang, T. Taira, M. Kaplitt, A. Rezai, J. Rumià, W. Gedroyc, K. Igase, H. Kishima, K. Yamada, H. Ohnishi, C. Halpern, Predictors of outcomes after focused ultrasound thalamotomy, Neurosurgery 87 (2) (2020) 229–237, https://doi.org/10.1093/neuros/nyz417.
- [22] V.T. Lehman, K.H. Lee, B.T. Klassen, D.J. Blezek, A. Goyal, B.R. Shah, K.R. Gorny, J. Huston, T.J. Kaufmann, MRI and tractography techniques to localize the ventral intermediate nucleus and dentatorubrothalamic tract for deep brain stimulation and MR-guided focused ultrasound: a narrative review and update, Neurosurg. Focus. 49 (1) (2020) E8, https://doi.org/10.3171/2020.4.FOCUS20170.
- [23] M. Ranjan, G.J.B. Elias, A. Boutet, J. Zhong, P. Chu, J. Germann, G.A. Devenyi, M. M. Chakravarty, A. Fasano, K. Hynynen, N. Lipsman, C. Hamani, W. Kucharczyk, M.L. Schwartz, A.M. Lozano, M. Hodaie, Tractography-based targeting of the ventral intermediate nucleus: accuracy and clinical utility in MRgFUS thalamotomy, J. Neurosurg. 133 (4) (2020) 1002–1009, https://doi.org/10.3171/2019.6.JNS19612.
- [24] H. Hori, T. Yamaguchi, Y. Konishi, T. Taira, Y. Muragaki, Correlation between fractional anisotropy changes in the targeted ventral intermediate nucleus and clinical outcome after transcranial MR-guided focused ultrasound thalamotomy for essential tremor: results of a pilot study, J. Neurosurg. 132 (2) (2020) 568–573, https://doi.org/10.3171/2018.10.JNS18993.
- [25] V. Purrer, N. Upadhyay, V. Borger, C. Schmeel, H. Boecker, U. Wüllner, Structural and functional alterations in the gustatory network underlie taste disturbances after lesional tremor therapy with MRgFUS, J. Neurol. Neurosurg. Psychiatry 94 (12) (2023) 1–3, https://doi.org/10.1136/jnnp-2023-331324.
- [26] W.S. Tae, B.J. Ham, S.B. Pyun, S.H. Kang, B.J. Kim, Current clinical applications of diffusion-tensor imaging in neurological disorders, J. Clin. Neurol. (Seoul, Korea) 14 (2) (2018) 129–140, https://doi.org/10.3988/jcn.2018.14.2.129.
- [27] S.-K. Song, J. Yoshino, T.Q. Le, S.-J. Lin, S.-W. Sun, A.H. Cross, R.C. Armstrong, Demyelination increases radial diffusivity in corpus callosum of mouse brain, NeuroImage 26 (1) (2005) 132–140, https://doi.org/10.1016/j. neuroimage.2005.01.028.
- [28] S.-W. Sun, H.-F. Liang, A.H. Cross, S.-K. Song, Evolving Wallerian degeneration after transient retinal ischemia in mice characterized by diffusion tensor imaging, NeuroImage 40 (1) (2008) 1–10, https://doi.org/10.1016/j. neuroimage.2007.11.049.
- [29] D.K. Jones, T.R. Knösche, R. Turner, White matter integrity, fiber count, and other fallacies: the do's and don'ts of diffusion MRI, NeuroImage 73 (2013) 239–254, https://doi.org/10.1016/j.neuroimage.2012.06.081.
- [30] G.P. Winston, J. Stretton, M.K. Sidhu, M.R. Symms, J.S. Duncan, Progressive white matter changes following anterior temporal lobe resection for epilepsy, NeuroImage. Clin. 4 (2014) 190–200, https://doi.org/10.1016/j.nicl.2013.12.004.
- [31] M. Wintermark, D.S. Huss, B.B. Shah, N. Tustison, T.J. Druzgal, N. Kassell, W. J. Elias, Thalamic connectivity in patients with essential tremor treated with MR imaging-guided focused ultrasound: in vivo fiber tracking by using diffusion-tensor MR imaging, Radiology 272 (1) (2014) 202–209, https://doi.org/10.1148/radiol_14132112
- [32] K. Bhatia, P. Bain, N. Bajaj, R. Elble, M. Hallett, E. Louis, J. Raethjen, M. Stamelou, C. Testa, G. Deuschl, Consensus statement on the classification of tremors. From the task force on tremor of the International Parkinson and Movement Disorder Society, Mov. Disord. 33 (1) (2018), https://doi.org/10.1002/mds.27121.
- [33] V.C. Keil, V. Borger, V. Purrer, S.F. Groetz, L. Scheef, H. Boecker, H.H. Schild, C. Kindler, A. Schmitt, L. Solymosi, U. Wüllner, C.C. Pieper, MRI follow-up after magnetic resonance-guided focused ultrasound for non-invasive thalamotomy: the neuroradiologist's perspective, Neuroradiology 62 (9) (2020) 1111–1122, https:// doi.org/10.1007/s00234-020-02433-9.
- [34] E.D.R. Pohl, N. Upadhyay, X. Kobeleva, V. Purrer, A. Maurer, V.C. Keil, C. Kindler, V. Borger, C.C. Pieper, S. Groetz, L. Scheef, J. Maciaczyk, H. Schild, H. Vatter, T. Klockgether, A. Radbruch, U. Attenberger, U. Wüllner, H. Boecker, Coherent structural and functional network changes after thalamic lesions in essential tremor, Movement Disord. 37 (9) (2022) 1924–1929, https://doi.org/10.1002/mds.29130.
- [35] S. Fahn, E. Tolosa, C. Marin, Clinical Rating Scale for Tremor 2, 1988, pp. 271–280.
- [36] R. Elble, P. Bain, M. Forjaz, D. Haubenberger, C. Testa, C. Goetz, A. Leentjens, P. Martinez-Martin, A. Pavy-Le Traon, B. Post, C. Sampaio, G. Stebbins, D. Weintraub, A. Schrag, Task force report: scales for screening and evaluating tremor: critique and recommendations, Mov. Disord. 28 (13) (2013), https://doi. org/10.1002/mds.25648.
- [37] F. Ghielmetti, D. Aquino, N. Golfrè Andreasi, F. Mazzi, E. Greco, R. Cilia, E. De Martin, S. Rinaldo, M. Stanziano, V. Levi, A. Braccia, M. Marchetti, M.L. Fumagalli, G. Demichelis, F. Colucci, L.M. Romito, G. Devigili, A.E. Elia, V. Caldiera, R. Eleopra, Quantitative tractography-based evaluations in essential tremor patients after MRgFUS thalamotomy, Movem. Disord. Clin. Pract. (2024), https://doi.org/10.1002/mdc3.14219.
- [38] N. He, J. Langley, D.E. Huddleston, H. Ling, H. Xu, C. Liu, F. Yan, X.P. Hu, Improved neuroimaging atlas of the dentate nucleus, Cerebellum (London, England) 16 (5–6) (2017) 951–956, https://doi.org/10.1007/s12311-017-0872-7.

- [39] S. Mori, S. Wakana, L.M. Nagae-Poetscher, P.C.M. van Zijl, MRI atlas of human White matter, Am. J. Neuroradiol. 27 (6) (2006) 1384–1385.
- [40] G. Grabner, A.L. Janke, M.M. Budge, D. Smith, J. Pruessner, D.L. Collins, Symmetric Atlasing and model based segmentation: An application to the Hippocampus in older adults, in: R. Larsen, M. Nielsen, J. Sporring (Eds.), Medical Image Computing and Computer-Assisted Intervention – MICCAI 2006, Springer, 2006, pp. 58–66, https://doi.org/10.1007/11866763_8.
- [41] S. Nkomboni, F. Isbaine, R. Gross, N.A. Yong, L. Higginbotham, C. Esper, P. Aia, L. Scorr, S. Triche, C. Buetefisch, S. Miocinovic, R. Tripathi, High intensity focused ultrasound—volume of tissue ablation and correlation with tremor control (P3-3.015), Neurology 102 (17 supplement_1) (2024) 6743, https://doi.org/10.1212/WNL.0000000000206662.
- [42] A.N. Kapadia, G.J.B. Elias, A. Boutet, J. Germann, A. Pancholi, P. Chu, J. Zhong, A. Fasano, R. Munhoz, C. Chow, W. Kucharczyk, M.L. Schwartz, M. Hodaie, A. M. Lozano, Multimodal MRI for MRgFUS in essential tremor: Post-treatment radiological markers of clinical outcome, J. Neurol. Neurosurg. Psychiatry 91 (9) (2020) 921–927, https://doi.org/10.1136/jnnp-2020-322745.
- [43] M.G. Kendall, A new measure of rank correlation, Biometrika 30 (1/2) (1938) 81–93, https://doi.org/10.2307/2332226.
- [44] S. Arndt, C. Turvey, N.C. Andreasen, Correlating and predicting psychiatric symptom ratings: spearman's r versus Kendall's tau correlation, J. Psychiatr. Res. 33 (2) (1999) 97–104, https://doi.org/10.1016/s0022-3956(98)90046-2.
- [45] K. Kyle, J. Maller, Y. Barnett, B. Jonker, M. Barnett, A. D'Souza, F. Calamante, J. Maamary, J. Peters, C. Wang, S. Tisch, Tremor suppression following treatment with MRgFUS: skull density ratio consistency and degree of posterior dentatorubrothalamic tract lesioning predicts long-term clinical outcomes in essential tremor, Front. Neurol. 14 (2023), https://doi.org/10.3389/ fneur.2023.1129430.
- [46] T.R. Miller, J. Zhuo, H.M. Eisenberg, P.S. Fishman, E.R. Melhem, R. Gullapalli, D. Gandhi, Targeting of the dentato-rubro-thalamic tract for MR-guided focused

- ultrasound treatment of essential tremor, Neuroradiol. J. 32 (6) (2019) 401–407, https://doi.org/10.1177/1971400919870180.
- [47] A. Alexander, J. Lee, M. Lazar, A. Field, Diffusion tensor imaging of the brain, Neurotherap. J. Am. Soc. Exp. NeuroTherap. 4 (3) (2007), https://doi.org/ 10.1016/j.nurt.2007.05.011.
- [48] M.R. Walker, J. Zhong, A.C. Waspe, T. Looi, K. Piorkowska, C. Hawkins, J. M. Drake, M. Hodaie, Acute MR-guided high-intensity focused ultrasound lesion assessment using diffusion-weighted imaging and histological analysis, Front. Neurol. 10 (2019) 1069, https://doi.org/10.3389/fneur.2019.01069.
- [49] L.K.L. Oestreich, M.J. O'Sullivan, Transdiagnostic in vivo magnetic resonance imaging markers of neuroinflammation, Biol. Psychiatry Cognit. Neurosci. Neuroimag. 7 (7) (2022) 638–658, https://doi.org/10.1016/j.bpsc.2022.01.003.
- [50] S.E. Blitz, M. Torre, M.M. Chua, S.L. Christie, N.J. McDannold, G.R. Cosgrove, Focused ultrasound thalamotomy: correlation of postoperative imaging with neuropathological findings, Stereotact. Funct. Neurosurg. 101 (1) (2023) 60–67, https://doi.org/10.1159/000527269.
- [51] S. Koga, M. Ishaque, W. Jeffrey Elias, B.B. Shah, A. Murakami, D.W. Dickson, Neuropathology of Parkinson's disease after focused ultrasound thalamotomy, NPJ Parkinson's Disease 8 (1) (2022) 1–6, https://doi.org/10.1038/s41531-022-00319-6.
- [52] L. Conforti, J. Gilley, M.P. Coleman, Wallerian degeneration: an emerging axon death pathway linking injury and disease, Nat. Rev. Neurosci. 15 (6) (2014) 394–409, https://doi.org/10.1038/nrn3680.
- [53] N. Solowij, A. Zalesky, V. Lorenzetti, M. Yücel, Chapter 40—Chronic Cannabis use and axonal Fiber connectivity, in: V.R. Preedy (Ed.), Handbook of Cannabis and Related Pathologies, Academic Press, 2017, pp. 391–400, https://doi.org/ 10.1016/B978-0-12-800756-3.00046-6.
- [54] P.J. Winklewski, A. Sabisz, P. Naumczyk, K. Jodzio, E. Szurowska, A. Szarmach, Understanding the physiopathology behind axial and radial diffusivity changes—What do we know? Front. Neurol. 9 (2018) 92, https://doi.org/10.3389/ fneur 2018 00092